Normal Monthly Wind Stress Over the World Ocean with Error Estimates

SOL HELLERMAN[1] AND MEL ROSENSTEIN[2]

Princeton University, Princeton, NJ 08540

(Manuscript received 29 November 1982, in final form 24 March 1983)

ABSTRACT

Over 35 million surface observations covering the world ocean from 1870–1976 have been processed for the purpose of calculating monthly normals and standard errors of the eastward and northward components of the wind stress and work done by the winds in the lower 10 m of the atmosphere. The fields are intended to serve as boundary conditions for models of the ocean circulation. Wind and air-minus-sea temperatures are calculated in a form suitable for determining stress by any bulk aerodynamics model in which the drag coefficient can be represented by six or less coefficients of a second-degree polynomial in wind speed and stability. The particular case of the wind speed and stability dependent drag coefficient discussed by Bunker is selected for analysis. January and July charts of wind stress, curl of the wind stress, mass transport streamfunction, divergence of the Ekman transport and the rate of mechanical energy transfer are illustrated and discussed.

1. Introduction

Following Sverdrup's (1947) pioneering work relating mass transport streamfunction to the curl of the wind stress, the Scripps Institute of Oceanography made the first concerted effort to calculate the large scale wind stress τ over the North Pacific Ocean in 1948 and followed with similar calculations for the North Atlantic ocean in 1950. These studies were based on U.S. Navy Hydrographic Office Pilot Charts consisting of wind roses constructed from wind reports in a 5° latitude by 5° longitude box. Information provided by the wind rose were mean wind speeds and direction frequencies from each of sixteen directions. A Gaussian distribution of wind speed centered on the mean was assumed for low latitudes and a skewed distribution, suggested from the statistics of available data, assumed for high latitudes. Hidaka (1958) extended this work to the South Pacific, South Atlantic and Indian Oceans.

In these and succeeding studies τ has been calculated by means of the quadratic bulk aerodynamic formulation,

$$|\tau| = \rho C_D(u^2 + v^2),$$

$|\tau|$ being the modulus of the stress vector, ρ the air density at the atmosphere–ocean interface, and u and v are the eastward and northward components of 10 m wind velocity. In the earlier studies, the nondimensional drag coefficient C_D, was taken to be 0.8×10^{-3} for wind speed < 6.7 m s^{-1} and 2.6×10^{-3} for wind speed > 6.7 m s^{-1}. Later studies used a wide variety of functional forms of C_D.

Hellerman (1967) recalculated τ on the world ocean using wind rose data from the U.S. Navy Hydrographic Office Marine Climatic Atlas of the World. These wind roses included speed frequencies for each direction in speed bands roughly 2 Beaufort numbers wide, partially obviating the need for speed frequency assumptions. A wind speed dependent C_D with gradual transition from 0.85×10^{-3} to 2.43×10^{-3} in the vicinity of 6.7 m s^{-1} was used. Most wind roses contain large amounts of historical data but there were only about 3800 wind roses for twelve months for the entire world ocean. This data set was therefore supplemented with Pilot Chart data and only seasonal stresses were calculated.

In more recent times, millions of surface observations collected by the National Climatic Center in Asheville, NC, designated TDF-11, have become available. Wyrtki and Meyers (1976) processed a portion of TDF-11 involving over five million observations taken from 1945 to 1970, to derive wind stress for the Pacific Ocean from 30°S to 30°N. Bunker (1976) processed over 12 million observations for the Atlantic Ocean for the period 1941–72. Hastenrath and Lamb (1977) used the 1911–70 portion of TDF-11 to find normals over the tropical Atlantic and eastern Pacific Oceans.

In connection with modeling the ocean circulation, there is a need for a consistent global wind stress data set. In this study we use the entire TDF-11 for the world ocean. The data is grouped by month for the 106 year period from 1870–1976 into 2° latitude by 2° longitude boxes, subjectively chosen as a compro-

[1] Geophysical Fluid Dynamics Program.
[2] Geophysical Fluid Dynamics Laboratory/NOAA.

TABLE 1. Number of observations ($\times 10^6$).

	Jan	Feb	Mar	Apr	May	Jun	Jul	Aug	Sep	Oct	Nov	Dec	Annual
Northern Hemisphere	2.3	2.2	2.5	2.3	2.5	2.4	2.5	2.5	2.4	2.4	2.4	2.3	28.7
Southern Hemisphere	0.6	0.5	0.6	0.5	0.6	0.5	0.6	0.6	0.5	0.5	0.6	0.6	6.7
World	2.9	2.7	3.1	2.8	3.1	2.9	3.1	3.1	2.9	2.9	3.0	2.9	35.4

mise between larger boxes that would be needed in data sparse regions and smaller boxes that would suffice in data rich regions. It is our purpose to determine global monthly normals of τ and rate of wind work in the lower atmosphere W.

From the vector τ, a function of $|\mathbf{v}|^2$, estimates can be made of surface drift, Ekman transport and pumping, and vertically integrated transports as approximated by the Sverdrup relation. The rate of wind work W, however, is proportional to the energy available for bringing heat and mechanical energy to subsurface layers and is proportional to $|\mathbf{v}|^3$. Processing individual observations affords the opportunity to calculate this important quantity explicitly, which can otherwise only be approximated from resultant winds.

Various constant values and functional forms of C_D have been suggested for use in the bulk aerodynamic formulation, and it is not a settled matter as to which is most appropriate for calculation of large scale τ. Processing TDF-11 for each suggested C_D would be tedious and prohibitively costly. Therefore the terms of $|\tau|$ and $|\tau|^2$ calculated by the bulk aerodynamic formulation, with a C_D approximated by a polynomial of second degree in wind speed and stability were stored on tape. The six or less coefficients required to describe the C_D polynomial are then all that are required to recalculate $|\tau|$ and $|\tau|^2$ for alternate C_D's. For this study the wind speed and stability dependent C_D of Bunker (1976, Table 2) was selected for analysis. The stability dependence of C_D is based on the work of Deardorff (1968) relating C_D to the Richardson number.

2. Data

TDF-11 is a historic data file of surface weather observations made at sea and arranged chronologically and by Marsden squares. Only the reports containing synoptic air and sea temperatures, as well as wind speed and direction, were selected for use in this study. The time and space distribution of these data are summarized in Table 1. The more expansive Southern Hemisphere oceans have less than one fourth the number of observations of the Northern Hemisphere oceans. The number of observations per 2° by 2° sector, for January and July are roughly contoured in Fig. 1. A notable feature of these charts is the characteristically narrow high density bands of the major commercial sea lanes.

The sparse TDF-11 data sample at high latitudes is supplemented in this study with wind-rose data from the Arctic and Antarctic (*Oceanographic Atlases of the Polar Seas of the U.S. Navy Hydrographic Office, 1957–1958*) and a neutral stability was assumed for these data. To assess the role of stability on $|\tau|$ we calculated the τ^x field with a wind speed and stability dependent C_D and with a wind speed (but neutrally stable) dependent C_D, and subtracted the latter from the former. The differences in τ^x for January and July are shown in Fig. 2. From these charts it is clear that the instability of winter cold air outbreaks from Asia and North America result in significantly higher τ^x than would be the case for a neutrally stable atmosphere. In this report therefore, there may be a bias toward lower stresses in polar regions when the air is colder than the underlying leeds and ice.

Stress components, energy transfer, and their squares in polynomial form are described as follows. With TDF-11 data we calculate

$$\tau^x = \rho C_D u(u^2 + v^2)^{1/2}, \tag{1}$$

$$\tau^y = \rho C_D v(u^2 + v^2)^{1/2}, \tag{2}$$

$$W = \rho C_D[(u^2 + v^2)^{1/2}]^3, \tag{3}$$

where τ^x and τ^y are exchanges between atmosphere and ocean of zonal and meridional momentum and W is the power of the wind in the atmospheric boundary layer; $\rho = 1.2 \times 10^{-3}$ g cm^{-3} is air density, C_D is the exchange coefficient for momentum, u and v are the eastward and northward components of wind velocity.

For this study C_D is considered to be a function of wind speed, $(u^2 + v^2)^{1/2}$, and of air minus sea temperature, $T_a - T_s$. It is approximated by the polynomial

$$C_D = \alpha_1 + \alpha_2(u^2 + v^2)^{1/2} + \alpha_3(T_a - T_s) + \alpha_4(u^2 + v^2) + \alpha_5(T_a - T_s)^2 + \alpha_6(u^2 + v^2)^{1/2}(T_a - T_s). \tag{4}$$

Let $(u^2 + v^2)^{1/2} = M$ and $T_a - T_s = \Delta T$. Then Eqs. (1), (2) and (3) may now be approximated by

$$\tau^x \approx \rho uM[\alpha_1 + \alpha_2 M + \alpha_3 \Delta T + \alpha_4 M^2 + \alpha_5(\Delta T)^2 + \alpha_6 M(\Delta T)], \tag{5}$$

$$\tau^y \approx \rho vM[\alpha_1 + \cdots + \alpha_6 M(\Delta T)], \tag{6}$$

$$W \approx \rho M^3[\alpha_1 + \cdots + \alpha_6 M(\Delta T)]. \tag{7}$$

In order to estimate errors, the variances of τ^x, τ^y and W are needed:

$$(\tau^x)^2 \approx \rho^2 u^2 M^2[\alpha_1^2 + 2\alpha_1\alpha_2 M + 2\alpha_1\alpha_3\Delta T + (2\alpha_1\alpha_4 + \alpha_2)^2 M^2 + (2\alpha_1\alpha_5 + \alpha_3)^2(\Delta T)^2 + 2(\alpha_1\alpha_6 + \alpha_2\alpha_3)M(\Delta T)^2 + (2\alpha_3\alpha_4 + \alpha_2\alpha_6) \times M^2\Delta T + 2\alpha_3\alpha_5(\Delta T)^3 + \alpha_4^2 M^4 + (2\alpha_4\alpha_5 + \alpha_6^2) \times M^2(\Delta T)^2 + 2\alpha_4\alpha_6 M^3(\Delta T) + \alpha_5^2(\Delta T)^4 + 2\alpha_5\alpha_6 M(\Delta T)^3], \quad (8)$$

$$(\tau^y)^2 \approx \rho^2 v^2 M^2[\alpha_1^2 + \cdots], \quad (9)$$

$$(W)^2 \approx \rho^2 M^6[\alpha_1^2 + \cdots]. \quad (10)$$

Monthly normals of the six terms of Eqs. (5), (6) and (7) required to calculate τ^x, τ^y and W, and the 15 terms of Eqs. (8), (9) and (10) required to calculate $(\tau^x)^2$, $(\tau^y)^2$ and W^2 for each 2° × 2° box of the world ocean are stored on tape. The monthly normals provide a very general basis for computing wind stress and wind work for any drag coefficient involving M and ΔT to second order. Bunker (1976) provides a table of drag coefficient as a function of wind speed and stability. To determine the drag coefficient formula equivalent to his table, six normal equations were formulated from the tabular values of $(u^2 + v^2)^{1/2}$ and ΔT and solved by least squares for the coefficients of the best fitting second-degree polynomial. The best fit is given by

$$C_D(M, \Delta T) = 0.934 \times 10^{-3} + 0.788 \times 10^{-4} M + 0.868 \times 10^{-4}\Delta T - 0.616 \times 10^{-6} M^2 - 0.120 \times 10^{-5}(T)^2 - 0.214 \times 10^{-5} M(\Delta T). \quad (11)$$

The tabular values and the least-squares fit to the tabular values are contoured in Fig. 3. It is clear that the best fit deviates little from the tabular values of the $(u^2 + v^2)^{1/2}$ and (ΔT) in the ranges of most observations.

For convenience of mapping and calculating integrals, it is desirable to interpolate from surrounding

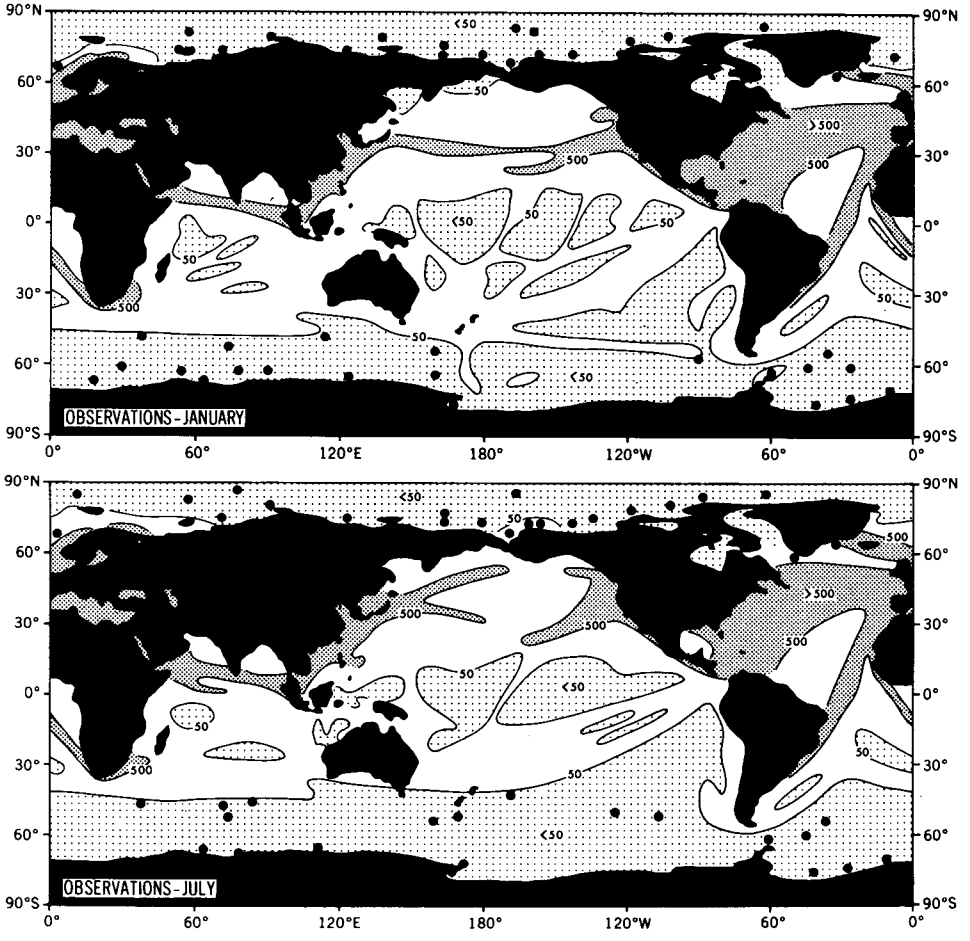

FIG. 1. Number of observations N per 2° latitude × 2° longitude box, smoothed; light shading for $N < 50$, no shading for $50 < N < 500$ and dark shading for $N > 500$. Heavy dots mark the locations for which supplemental data from the Arctic Atlases (U.S. Navy Hydrographic Office, 1958, 1959) for one or more months were used.

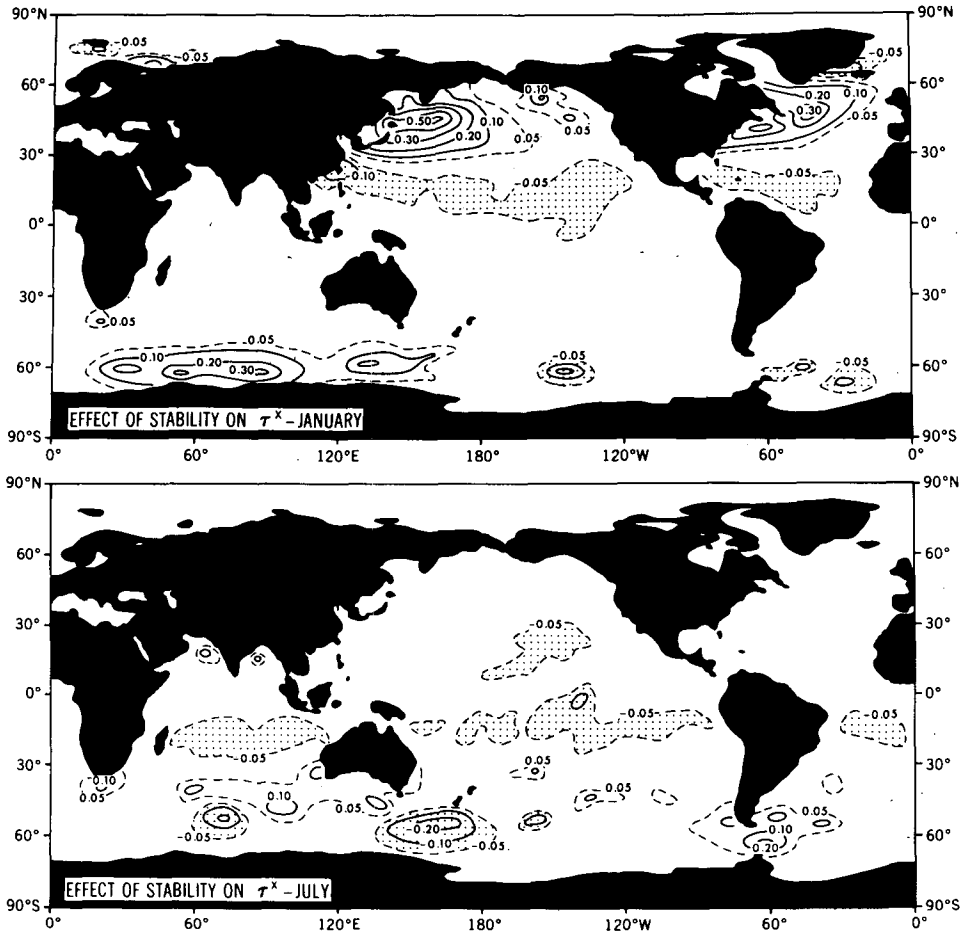

FIG. 2. The difference of τ^x (dyn cm^{-2}) calculated with a wind speed and stability dependent C_D, from τ^x calculated with the same wind speed dependent, but neutrally stable, C_D.

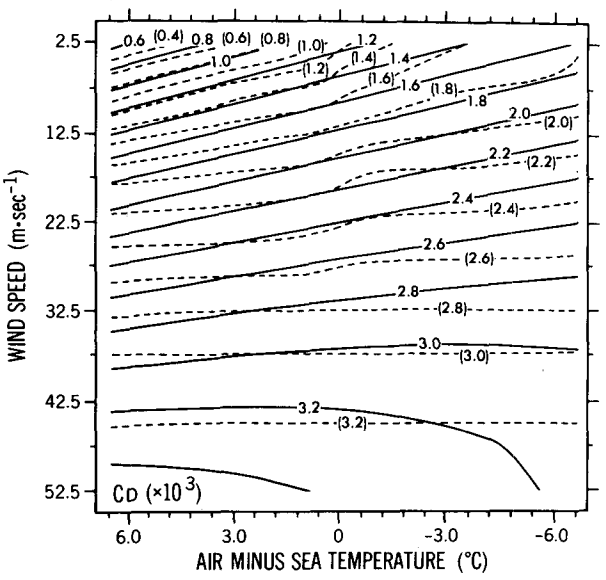

FIG. 3. Wind speed and stability dependent C_D from the tabular values of Bunker (1976) (dashed lines) and from a least-squares fit to the tabular values as used in this study (solid lines).

data boxes to the data deficient boxes, i.e., boxes with less than four observations. We solve $\nabla^2\phi = \sigma N^{-1/2} f(\phi - \phi^*)$ by relaxation, where ϕ are the interpolated and smoothed elements, ϕ^* are boundary values, i.e., means of ϕ in boxes that have data; $\sigma N^{-1/2}$ is a measure of uncertainty in ϕ^*, where σ is the standard deviation and N is the number of observations in a 2° × 2° box, and $f = 0.2$ is an arbitrary smoothing factor.

3. Analyses and Comparisons with Previous Work

a. *Wind stress*

Fig. 4 displays the January and July τ normals derived from the data and processing described above. A measure of confidence to be placed in the τ^x of these charts is shown in Fig. 5, which maps the standard error of the mean of τ^x, $\epsilon(\tau^x)$. Because of TDF-11, N is sufficiently large over most of the world ocean for $\epsilon(\tau^x)$ to be less than 0.1 dyn cm^{-2}. We note comparable $\epsilon(\tau^x)$ in the tropic Pacific region, where

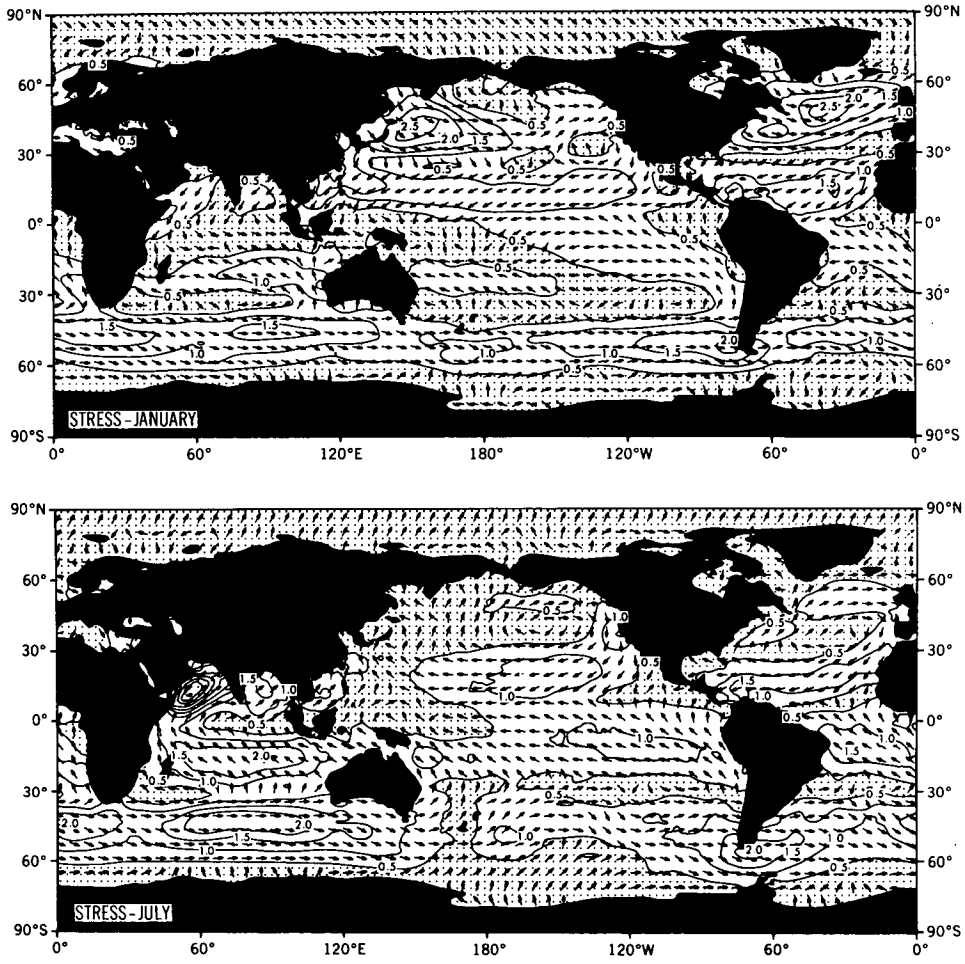

FIG. 4. Wind stress fields. Arrows indicate direction and contours the magnitude (dyn cm^{-2}) of the wind stress vectors. Shading marks magnitudes < 0.5 dyn cm^{-2}.

there are <50 observations per 2° box, as in the winter north Pacific and Atlantic regions where there are >500 observations per 2° box. The tropical Pacific is a region of low σ and the winter mid-latitude regions are regions of relatively high σ. On the other hand, $N < 50$ for the former and $N > 500$ for the latter regions, causing the $\epsilon(\tau^x)$ statistic to be comparable in the two regions.

In Fig. 6 the annual zonal means of τ^x of this study are shown and compared with that of the 1967 study. Though no error estimate was made for the earlier study, wind rose and Pilot Chart data were especially sparse at the high latitudes of the Southern Hemisphere, $\epsilon(\tau^x)$ for the present study over much of this region is about 0.5 dyn cm^{-2}.

We also calculated τ^x for the region of the Pacific Ocean and using the same $C_D = 1.5 \times 10^{-3}$ as was used by Wyrtki and Myers (1976). The results of the two calculations are compared in Fig. 7. The small difference in the results are mainly attributed to the different portions of the TDF-11 used and to the different methods of data grouping, Wyrtki and Myers having grouped the data in 2° latitude by 10° longitude boxes. These differences are apparently not significant compared to the differences in τ^x between that of the Wyrtki and Myers constant $C_D = 1.5 \times 10^{-3}$ study and that of the $C_D((u^2 + v^2)^{1/2}, \Delta T)$ of this study.

The patterns of the January τ^x of Bunker (1976) and of this study, shown in Fig. 8, are very similar, but the former τ^x are significantly larger. Bunker, for the most part, grouped the data into 2° by 5° boxes; otherwise the calculation procedures are similar for the two studies. The difference in τ^x, however, is mainly attributed to the smoothing procedures used. Bunker, working with an irregular grid, smoothed subjectively and maintained or only slightly truncated maxima and minima. In the stresses of this study, the smoothing factor of $f = 0.2$ (see Section 2a) produces about the same smoothness as appears on Bunker's charts but truncates maxima and minima significantly more.

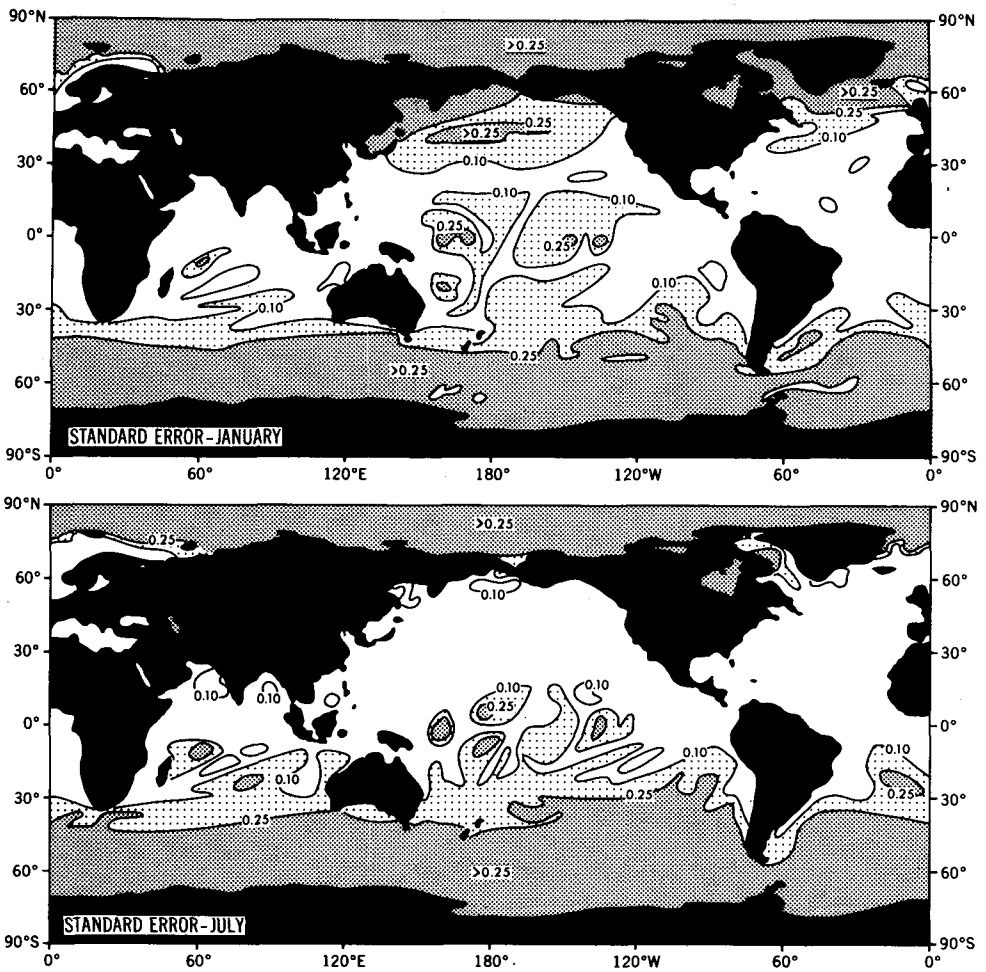

FIG. 5. Standard error of the mean of τ^x, $\epsilon(\tau^x)$, subjectively smoothed. No shading marks regions of $\epsilon(\tau^x) < 0.1$ dyn cm^{-2}, light shading marks regions of $0.1 < \epsilon(\tau^x) < 0.25$ dyn cm^{-2} and dark shading marks $\epsilon(\tau^x) > 0.25$ dyn cm^{-2}.

b. *Wind stress curl*

Because relatively large amplitude, small scale features tend to obscure the large scale patterns, some of the small scale features have been smoothed out of the January and July $\nabla \times \tau$ charts displayed in Fig. 9. Comparisons with $\nabla \times \tau$ charts of Hastenrath and Lamb (1977, chart 48) therefore show good large-scale pattern agreement but less than half of the $|\nabla \times \tau|$ value at the maxima and minima. The greater resolution of the Hastenrath and Lamb charts, also tend to yield higher $|\nabla \times \tau|$ values. Saunders (1976) demonstrates, in a North Atlantic test area, this dependence on $|\nabla \times \tau|$ on the data resolution.

A striking large scale feature of world $\nabla \times \tau$ fields is the system of 9 zonal belts (alternately positive and negative), interrupted and distorted by land masses, but quite distinguishable. Table 2 lists the approximate positions and extent of these zonal belts. Since we get approximate mass transport from the Sverdrup relation by integrating $\nabla \times \tau$ across the oceans zonally, the western parts of the $\nabla \times \tau$ belts for each ocean are roughly the locations of the major western boundary mass transports, and their sense is indicated by the sign of the $\nabla \times \tau$ belt.

c. *Mass transport and estimated error*

Mass transport stream function ψ (Fig. 10) was calculated from the Sverdrup relation

$$\psi = \int \frac{\nabla \times \tau}{\beta} dx + \text{constant},$$

where β is the y-derivative of the Coriolis parameter; the element of integration dx is taken along latitude lines from west to east, and a boundary value of $\psi = 0$ is assumed on land masses. The Sverdrup relation was developed for a steady state model and applies over long time-scales. In low latitudes "long" can be as short as a few months but this time-scale increases rapidly with latitude. Maps of Sverdrup transport for

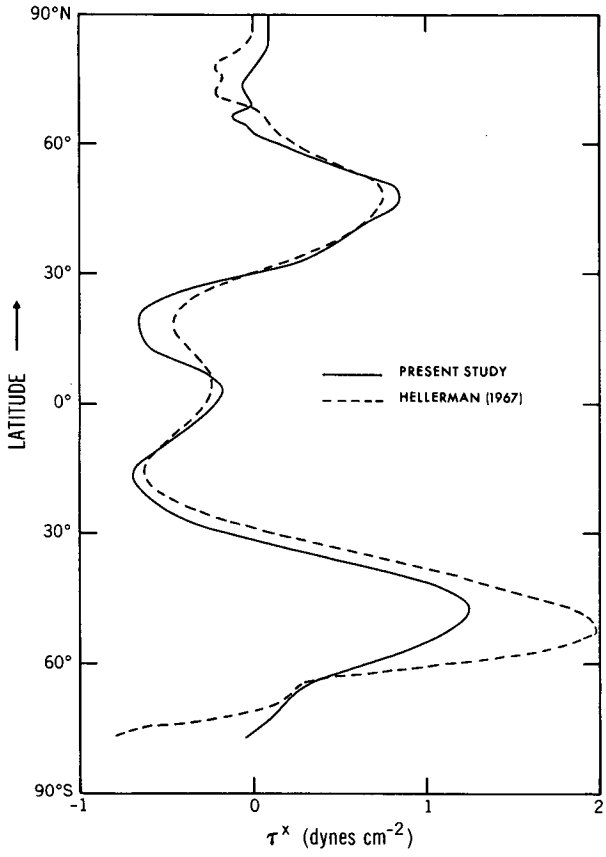

FIG. 6. Zonal means of annual τ^x (dyn cm^{-2}) from wind rose data of the Marine Climatic Atlases and Pilot Chart data of the U.S. Navy Hydrographic Office (dashed line) and zonal means of annual τ^x from TDF-11 data (solid line).

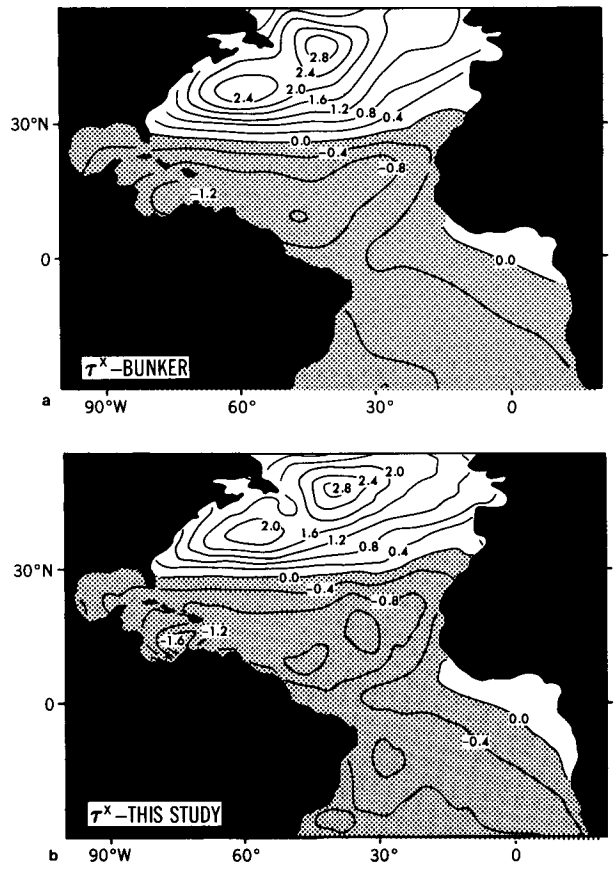

FIG. 8. (a) The January τ^x field (dyn cm^{-2}) for the 1941–72 portion of the TDF-11 file processed by Bunker (1976). (b) The January τ^x-field (dyn cm^{-2}) of this study for the Atlantic region.

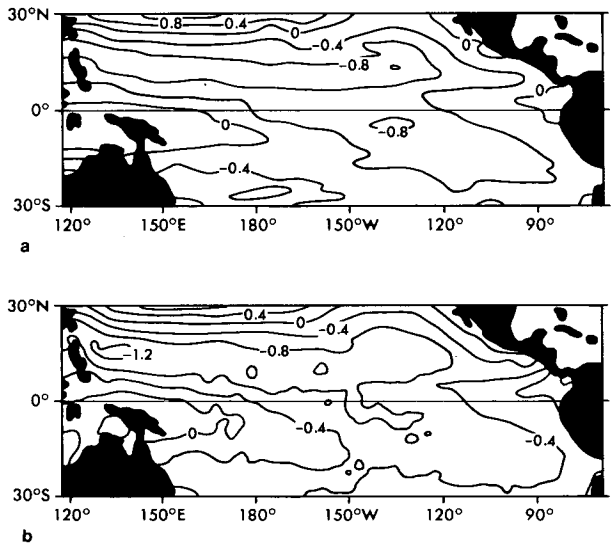

FIG. 7. (a) Pacific τ^x (dyn cm^{-2}) between 30°S and 30°N of Wyrtki and Meyers (1976) calculated with a constant $C_D = 1.5 \times 10^{-3}$ from the 1945–1970 portion of the TDF-11 file. (b) τ^x calculated as above, but from the entire TDF-11 file.

shorter periods may therefore be useful to assess at which latitudes Sverdrup theory is valid seasonally.

Mass transport stream function ψ is not evaluated in the landless Antarctic circumpolar region because of the lack of boundary values consistent with the arbitrary value of $\psi = 0$ on land. The ψ display is also omitted in some other regions where the estimated error is very large. For example, as the $\nabla \times \tau$ integration proceeds from the southern part of South America on a westward path uninterrupted by land through data sparse regions the accumulated estimated error becomes excessive.

The estimated error in ψ is

$$\epsilon(\psi) = 2(\beta N^{1/2})^{-1} \times \sum_{i=1}^{N} \left(\frac{\epsilon(\tau^y)}{a\Delta\lambda \cos\phi} + \frac{\epsilon(\tau^x)}{a\Delta\phi} \right) \Delta\lambda a \cos\phi, \quad (12)$$

where N is the number of statistically independent data points of the summation, $\epsilon(\tau^x)$ and $\epsilon(\tau^y)$ are the standard errors of τ^x and τ^y, respectively, a is the earth radius, and λ and ϕ are longitude and latitude,

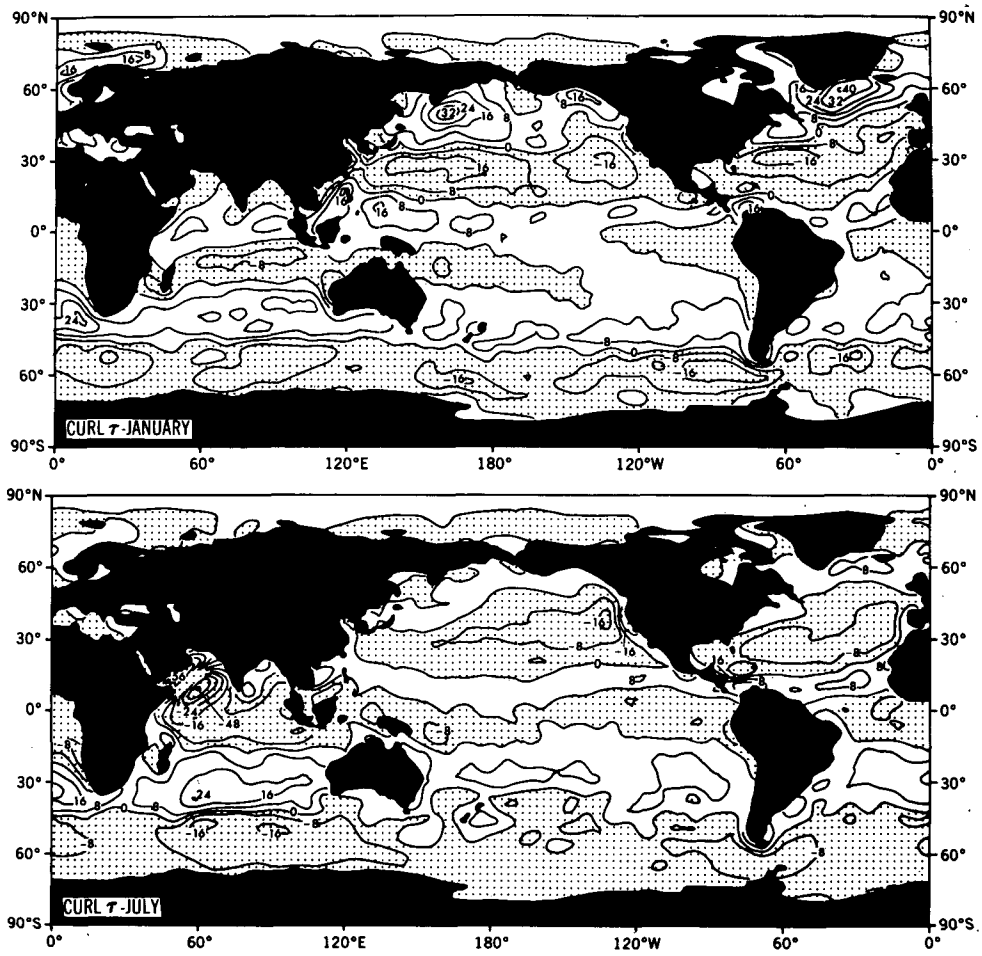

FIG. 9. Curl of the wind stress (10^{-9} dynes cm^{-3}) after a four-point smoothing was applied.

respectively. For calculating $\epsilon(\psi)$, data of each 2° × 2° box is considered an independent estimate. A value of 0.5 dyn cm^{-2} was subjectively chosen from Fig. 5 as representative of the standard error for 2°-boxes with no data. This value is a manually estimated fit for regions of low observation density, mainly high latitudes, and too large for the few 2°-boxes in regions of high observation density. A sample of $\epsilon(\tau^x)$ is displayed in Fig. 11. Welander (1959) calculated western boundary currents by the Sverdrup relation using the 5°-resolution annual stress data of Hidaka (1958) compiled from Pilot Charts. Table 3 summarizes western boundary current information from our Figs. 10 and 11 and from Welander (1959).

TABLE 2. Summary of January and July World Ocean zonal belts of curl of the wind stress. Mean latitude and mean width of World Ocean $\nabla \times \tau$ zones.

		January		July	
Zone	Sign	Mean latitude	Mean width (deg)	Mean latitude	Mean width (deg)
Arctic	+	85.0°N	10	84.0°N	12
Subarctic	−	76.0°N	8	73.0°N	10
North Temperate	+	56.0°N	32	56.0°N	24
North Subtropic	−	26.5°N	27	32.5°N	25
Tropic	+	4.0°N	18	13.0°N	12
South Subtropic	−	13.0°S	15	2.0°S	18
South Temperate	+	34.0°S	28	27.0°S	32
Subantarctic	−	60.0°S	24	58.5°S	31
Antarctic	+	74.0°S	4	75.0°S	2

The strength of the Sverdrup circulation in the subarctic gyre of the North Atlantic is approximately equal in strength to the subtropical gyre, while the subtropical gyre is much stronger relatively in the North Pacific. Note that the transport values of Welander (1959) are consistently low compared to those of the present study. The low estimates of wind driven circulation based on the wind data of Hidaka (1958) and the Scripps tables may have led to a somewhat exaggerated estimate of the discrepancy between mea-

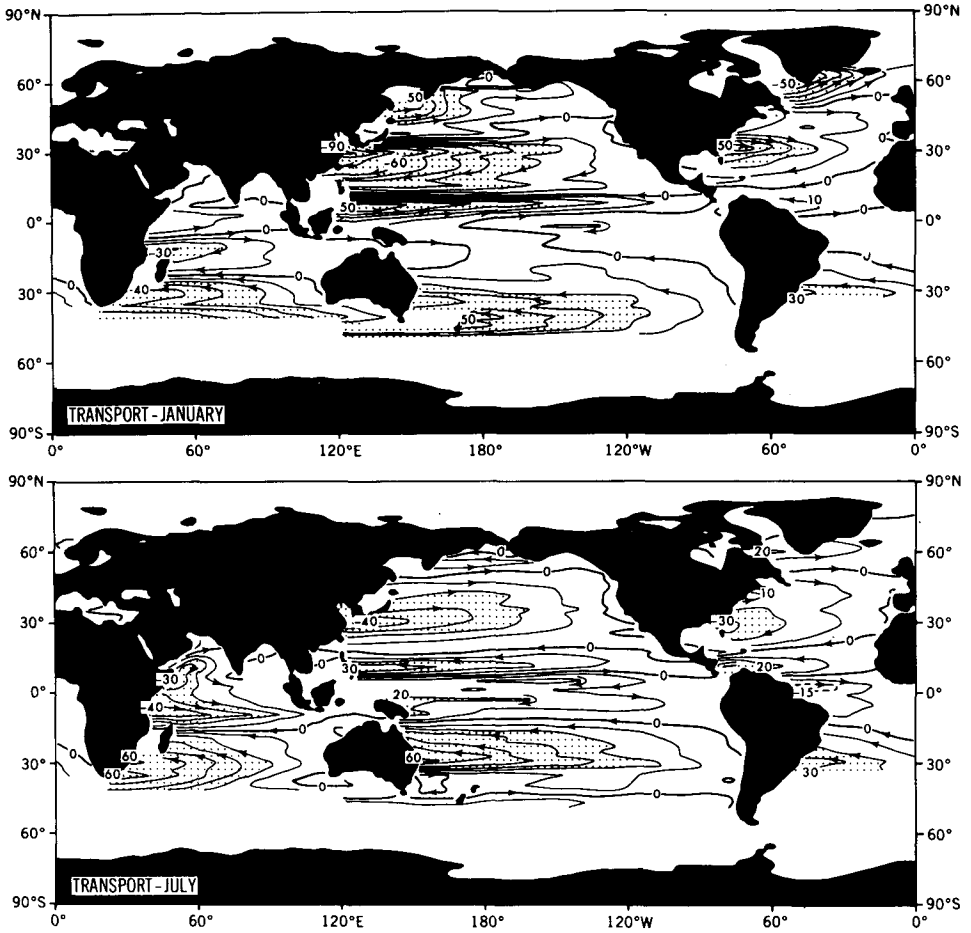

FIG. 10. Mass transport streamfunction ψ in g s^{-1} ($\times 10^{12}$) calculated from the Sverdrup relation. $|\psi| > 20 \times 10^{12}$ g s^{-1} is stippled.

sured values of western boundary current transport and Sverdrup theory.

The error estimates are unacceptably large in subarctic regions, but close to the 10% level at lower latitudes, sufficient for testing models of ocean circulation.

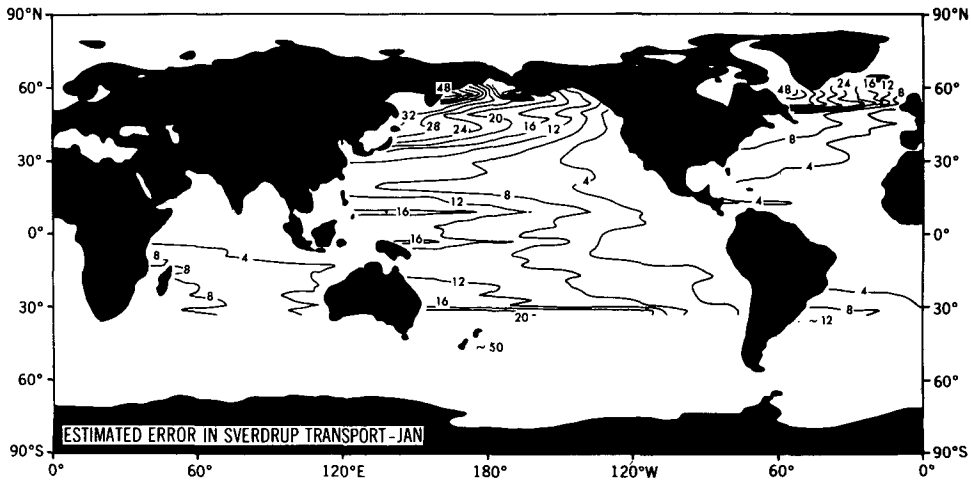

FIG. 11. The estimated error in Sverdrup transport in g s^{-1} ($\times 10^{12}$).

TABLE 3. Summary of the western boundary currents determined from the Sverdrup relation.

	Approximate location	ψ and $\epsilon(\psi)$ ($\times 10^{12}$ g s^{-1})	Annual ψ of Welander
		Atlantic Ocean	
Jan	55°N	50 ± 40	...
Jul	60°N	~20	
Jan	31°N	50 ± 7	23
Jul	28°N	30	
Jan	6°N	10 ± 3	7
Jul	11°N	40	
Jan	4°S	10 ± 4	9
Jul	1°N	15	
Jan	32°S	30 ± 12	28
Jul	30°S	30	
		Pacific Ocean	
Jan	48°N	50 ± 40	...
Jul	52°N	10	
Jan	30°N	90 ± 12	30
Jul	30°N	40	
Jan	6°N	50 ± 14	22
Jul	11°N	30	
Jan	...	...	10
Jul	5°S[1]	20	
Jan	35°S[2]	50 ± 50	28
Jul	30°S[3]	60	
		Indian Ocean	
Jan	0°	10 ± 3[4]	...
Jul	5°N	30	
Jan	13°S	30 ± 8	22
Jul	8°S	40	
Jan	32°S	40 ± 8	50
Jul	32°S	60	

[1] East of New Guinea.
[2] East of New Zealand.
[3] East of Australia.
[4] Note direction reversal between Jan and Jul.

d. Divergence of the Ekman transport

Divergence of the Ekman transport is a large component of ocean welling, defined as

$$\nabla \cdot \mathbf{V}_\epsilon = (af)^{-1}\left(\frac{1}{\cos\phi}\frac{\partial \tau^\phi}{\partial \lambda} - \frac{\partial \tau^\lambda}{\partial \phi} + \frac{\tau^\lambda}{\sin\phi\cos\phi}\right),$$

where f is the Coriolis parameter and the other symbols are as previously defined; $\nabla \cdot \mathbf{V}_\epsilon$ for January and July is shown in Fig. 12.

We get a component of coastal welling at points adjacent to land using the boundary condition $\tau^x = \tau^y = 0$. This local welling may be of opposite sign to the large scale welling in which it is embedded.

We note a shifting of the zero welling contour of midlatitudes 9° from winter to summer, from 39° to 48°N and 39° to 48°S. The positive $\nabla \cdot \mathbf{V}_\epsilon$ of the tropic–subtropic region expands and attains a maximum value in summer while the midlatitude positive $\nabla \cdot \mathbf{V}_\epsilon$ region shrinks and weakens.

In a separate study, examination of the time dependence of the zonal means of $\nabla \cdot \mathbf{V}_\epsilon$ near the equator reveals distinct semiannual maxima in April and October and minima in January and July. The dates of maxima, less ~15 to 30 days lag, correspond to the dates when the sun is overhead, and the dates, less lag, of minima correspond to the dates of lowest sun angle.

e. Rate of wind work in the lower atmosphere

A knowledge of the rate of mechanical energy transfer between atmosphere and ocean is essential for an accounting of the energy balance in the mixed layer. By mechanical stirring, the center of gravity of the upper ocean is raised as the warmer surface waters are forced to subsurface layers. Heat storage capacity, a major influence on climate, is thus enhanced.

A small fraction of the kinetic energy of the lower atmosphere enters the oceans as available kinetic energy, but the exact relationship is poorly understood. According to an estimate of Lueck (1982), based on a model of Richman and Garrett (1977), the rate of kinetic energy input on a large scale is $\sim 0.1W$. With this estimate in mind, the charts of Fig. 13 provide a global view of the wind energy available for mechanical stirring of the upper ocean.

Regions with largest available wind energy for ocean stirring occur in the stormy winter westerlies of the North Atlantic and Pacific Oceans, the summer monsoon of the Arabian Sea and the winter westerlies of the Antarctic circumpolar current region; 0.600 W, 0.475 W, 0.375 W and 0.350 W m^{-2}, respectively, as shown in Fig. 13. Not surprisingly, the largest values of W do not coincide with the largest stresses. A world ocean maximum stress of ~4.5 dyn cm^{-2} occurs in the Arabian Sea summer monsoon where winds hardly vary in direction, whereas the stresses of the January North Atlantic and North Pacific Oceans, where wind direction varies considerably with the passage of storms, are ~2.5 dyn cm^{-2}.

As a function of $|\mathbf{v}|^3$, W is underestimated because it is common practice to report estimated average wind speeds over a few seconds time interval. Thus, a wind speed report of 20 m s^{-1}, representing an average of 15, 20 and 25 m s^{-1} winds of equal duration will result in an underestimation of W by 12.5%; $|\tau|$, a function of $|\mathbf{v}|^2$, is also underestimated

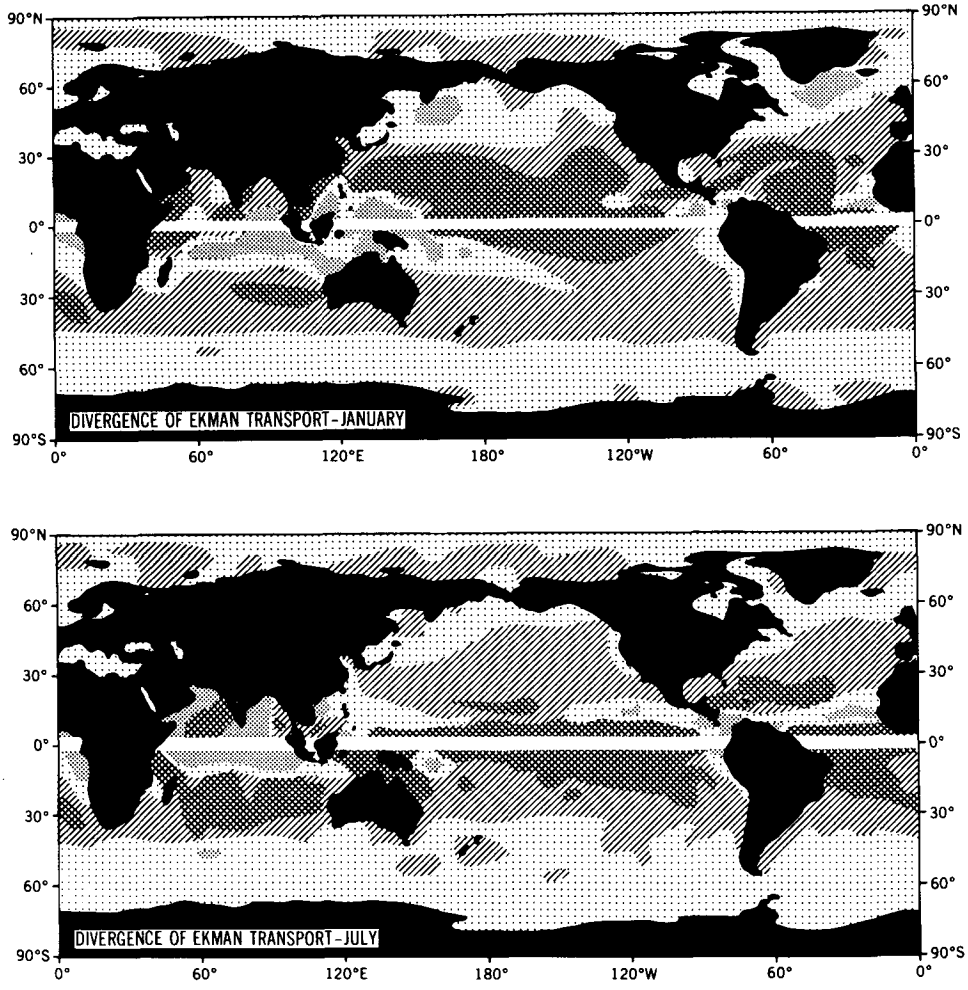

FIG. 12. Divergence of Ekman transport. Cross hatching covers areas of $\nabla \cdot \mathbf{V}_e < -20 \times 10^{-5}$ cm s^{-1} indicating downwelling of ~20 or more cm day^{-1}. Slant hatching covers downwelling areas of about 0 to 20 cm day^{-1}. Light stippling covers upwelling areas of about 0 to 20 cm day^{-1}, and dense stippling covers areas of $\nabla \cdot \mathbf{V}_e > 20 \times 10^{-5}$ cm s^{-1}, i.e., areas of upwelling of ~20 or more cm day^{-1}.

for the same reasons. For the above example of a reported wind speed of 20 m s^{-1} the underestimation in $|\tau|$ is about 4%.

4. Conclusion

Due to the vital role of the τ boundary condition in ocean dynamics, it is important that global τ-fields be updated with the best information available. As such, TDE-11 is a sufficiently dense and suitable data set for the calculation of monthly normals of τ in a 2°-resolution for the World Ocean. The C_D most frequently used in the bulk formula is either C_D as a constant, a function of wind speed alone or a function of wind speed and stability. We have processed the data so that any of these forms of C_D may be used to calculate τ, $\epsilon(\tau)$ and W. Sample charts of normal monthly wind stress and estimated errors, curl of the wind stress, mass transport stream function, divergence of the Ekman transport and rate of wind work in the lower atmosphere for a particular $C_D(u^2 + v^2)^{1/2}, \Delta T)$ are displayed and some large scale features noted. The tapes containing the τ-data for the particular C_D of this study, or the quantities required to calculate τ as a function of other C_D's will be made available by GFDL, upon request, for further investigation.

Basic data for this study are more voluminous than that of previous large-scale studies, making possible data analyses with higher confidence limits (and of smaller scales). Further additions to the data set will increase our confidence in the derived large-scale stress fields, however, with diminishing benefits for the effort expended. The stress tabulations of this study may be the best that can be done until wind

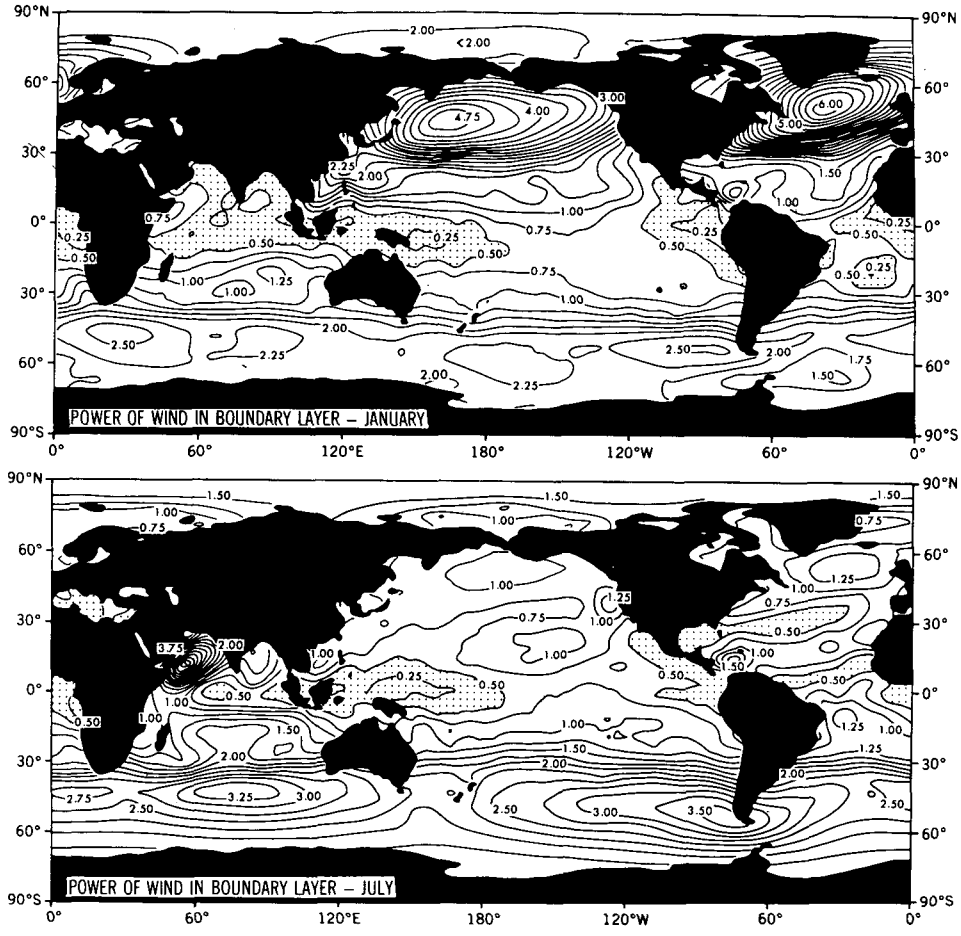

FIG. 13. Power of the winds in the atmospheric boundary layer W (W m^{-2}); $\sim 0.1W$ passes through the atmosphere–ocean interface.

stress measurements from satellites become available for longer periods.

Acknowledgments. The authors gratefully acknowledge the keen interest, suggestions and encouragement received from Dr. Kirk Bryan and Dr. Abraham Oort throughout this study; also the assistance of Betty Williams, Martha Jackson, and Phil Tunison and staff in the preparation of the manuscript. Support was received from GFDL/NOAA and NSF under Grant OCE8110155.

REFERENCES

Bunker, A. F., 1976: Computations of surface energy flux and annual air–sea interaction cycles of the North Atlantic Ocean. *Mon. Wea. Rev.*, **104,** 1122–1140.

Deardorff, J. W., 1968: Dependence of air–sea transfer coefficients on bulk stability. *J. Geophys. Res.*, **73,** 2549–2557.

Hastenrath, S., and P. J. Lamb, 1977: *Climatic Atlas of the Tropical Atlantic and Eastern Pacific Ocean.* University of Wisconsin Press.

Hellerman, S., 1967: An updated estimate of the wind stress in the World Ocean. *Mon. Wea. Rev.*, **95,** 607–626 (with corrected tables in **96,** 62–74).

Hidaka, K., 1958: Computation of the wind stresses over the oceans. *Rec. Oceanogr. Works Japan,*, **4,** 77–123.

Lueck, R. G., 1982: On the production and dissipation of mechanical energy in the ocean. (Submitted to *J. Geophys. Res.*)

Richman, J., and C. Garrett, 1977: The transfer of energy and momentum by the wind to the surface of the mixed layer. *J. Phys. Oceanogr.*, **7,** 876–881.

Saunders, P. M., 1976: On the uncertainty of wind stress curl calculations. *J. Mar. Res.*, **34,** 155–160.

Sverdrup, H. U., 1947: Wind-driven currents in a baroclinic ocean, with application to the equatorial currents of the eastern Pacific. *Proc. Nat. Acad. Sci. U.S.A.*, **33,** 318–326.

U.S. Navy Hydrographic Office, *Oceanographic Atlas of the Polar Seas.* Parts I and II, 1958, 1959: H.O. Pub. No. 705, Washington, DC.

Welander, P., 1959: On the vertically integrated mass transport in the oceans. *The Atmosphere and the Sea in Motion.* B. Bolin, Ed., Rockefeller Inst. Press and Oxford Univ. Press, 95–101.

Wyrtki, K., and G. Meyers, 1976: The trade wind field over the Pacific Ocean. *J. Appl. Meteor.*, **15,** 698–704.